A Complete Average Value Model of Modular Multilevel Converter

Jinling Qi[1], Haihao Jiang[2], Weixing Li[1], Boon-Teck Ooi[2]
Harbin Institute of Technology[1], McGill University[2]
China[1], Canada[2]

SUMMARY

Compared with the conventional line commutated converters (LCCs) based high voltage direct current (HVDC), the voltage source converters (VSCs) based HVDC has more wide applications, due to the advantages such as advanced controllability and reliability. Many topologies are proposed for the VSC-HVDC system, among them the modular multilevel converter (MMC) is the most promising one firstly proposed by Professor Marquardt of Universität der Bundeswehr München. Recently, the HVDC transmission based on MMC has been selected as the best solution for long-distance and high-power transmission. The MMC consists of massive submodules (SMs) for the high voltage applications. Each SM consists of several nonlinear components, such as the insulated-gate bipolar transistors (IGBTs). The detailed MMC model needs to model all the components. To simulate the detailed MMC model considering all the nonlinear components is time consuming and unpractical. Therefore, it is of great significance to develop a simple and accurate MMC model.
In this paper, the operating conditions of MMC are analyzed, including the startup process and normal operation. The equivalent circuits of MMC under different operating scenarios are established in the following. Based on the equivalent circuits of MMC, the ordinary differential equations considering the MMC internal variables, i.e., total capacitor voltage and the difference current are derived by applying the Kirchhoff's voltage law (KVL). In this case, the detailed SM is simplified for the modeling of MMC. Based on above analysis, an average value MMC model is developed which is composed of three controlled voltage sources to represent its ac-side and one controlled voltage source to represent its dc-side. The magnitude of the controlled voltage source is determined by continuous updating variables value through solving the ordinary differential equations. To validate the proposed average value model, several simulation tests are conducted and compared between the proposed model and detailed model in PSCAD/EMTDC, including the startup process, steady-state operation and circulating current suppression, based on a back to back MMC-HVDC system. During the startup process, the charging response of the proposed model follows the detailed model closely for both uncontrolled pre-charge process and controlled pre-charge process. Same conclusion applied to the steady-state operation. In order to show that the proposed model could also be used for the purpose of controller design, a circulating current suppression control (CCSC) strategy is applied to both the detailed MMC model and the proposed average value model. The simulation results show that the CCSC can suppress the circulating current effectively. Meanwhile, the comparison results between two models also validate the proposed average value MMC model. Since the proposed average value MMC model shows the great performance on computational speed and model accuracy, it is feasible for the simulation of large scale MMC-HVDC system and multi-terminal direct current (MTDC) grids.

jinling.qi@mail.mcgill.ca, hit_qijl@126.com

KEYWORDS

modular multilevel converter (MMC), average value model, electromagnetic transient (EMT) simulation.

1 Introduction

With the expanding of voltage level and power demand, modular multilevel converter (MMC) appears as a proper selection in high voltage direct current (HVDC) applications [1]. The MMC includes a large number of power semiconductor devices. To model the MMC system based on the full physics devices is unpractical for electromagnetic transient (EMT) simulation. To address this issue, many studies have been conducted for the accurate and efficient MMC model. Among these models, the average value model (AVM) attracts wide attention for its excellent computational efficiency.
The AVM is able to reproduce the averaged switching response while assuming that the voltages among the submodules (SMs) are balanced perfectly [2]. In [3]-[4], several AVMs are developed by deriving the mathematical expressions of MMC. However, only steady-state characteristics of MMC can be illustrated. In [5], each arm of MMC is represented as a controlled voltage source, and the dc-side model is represented as a controlled current source paralleled with an equivalent capacitor based on the principle of power balance. To further simplify the MMC model, the ac-side model in [5] is described as a three-phase controlled ac voltage source [6]. Though these models show excellent computational performance, they cannot be applied to investigate the startup process. In [7]-[8], additional diodes and ideal switches are introduced in the MMC model to connect the ac-side and dc-side of MMC under the startup process. Nevertheless, it requires the corporation of the several switches to mimic the characteristics of MMC under the startup process, which increases the complexity of the model as well as the calculation time. To fill the gap, a complete and computational efficient AVM for MMC including startup process and steady state operation has been proposed in this paper.

2 Modeling of MMC

To develop the complete average value MMC model, the startup process and normal operation of MMC are analyzed and modeled.

2.1 Startup Process

The startup process consists of two steps: uncontrolled pre-charge and controlled pre-charge.

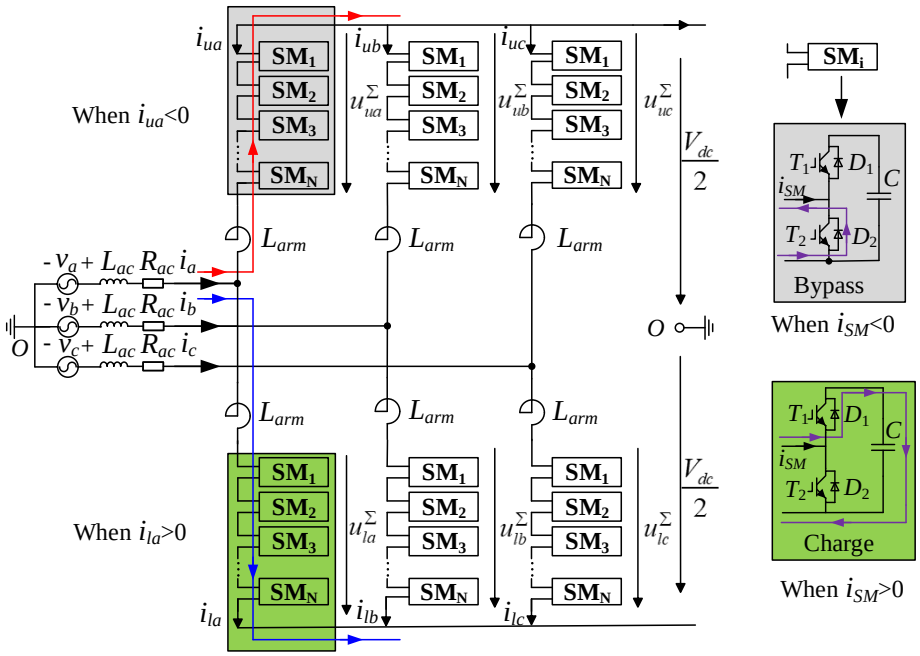

Fig.1. Schematic diagram of HBSM-MMC system.

In the beginning of the simulation, the MMC is blocked. The capacitors are charging through the freewheeling diodes of the SMs by the three-phase ac source. This stage is identified as uncontrolled pre-charge process. The schematic diagram of half-bridge SM (HBSM) based MMC is shown in Fig. 1. The v_j and i_j stand for the ac voltage and the current of phase j (j=a,b,c). i_{kj} presents the current in the k arm of phase j, k=u, l. The subscripts u and l represent the upper and lower arm respectively. u_{kj}^{Σ} is the total capacitor voltage in k arm of phase j. V_{dc} is the dc-link voltage of the MMC. R_{ac} and L_{ac} are the resistance and inductance of the ac side, and L_{arm} is the inductance of the MMC arm. SM$_i$ is the ith SM of each arm, i=1,2, …, N, while N is the number of SMs per arm. T_1 and T_2 are two IGBTs while D_1 and D_2 are the freewheeling diodes. C is the capacitance of each SM. i_{SM} is the injection current of SM. The black arrows in Fig. 1 present the positive current flow direction.

For each blocked SM, when i_{SM} is positive, the SM capacitor is charging, as shown in the green block in Fig. 1. When i_{SM} is negative, the SM capacitor is bypassed, as shown in the grey block in Fig. 1. Taking phase-a as an example, when i_{ua} is negative, all the N SMs capacitors of the upper arm are bypassed. When i_{la} is positive, all the N SMs capacitors of the lower arm are charging. The SM capacitor charging state of phase-a leg (upper arm and lower arm) is also shown in Fig. 1. To develop the AVM of MMC under this stage, a charging index s_{kj} decided by arm current flow direction is defined to represent the charging state:

$$s_{kj}=\begin{cases}1, & i_{kj}>0\\ 0, & i_{kj}\le 0\end{cases}, k=u,l \text{ and } j=a,b,c \tag{1}$$

where s_{kj}=1 means that all the N SMs capacitors in the arm are charging while s_{kj}=0 means bypassed. The total SM voltage in the k arm of phase j u_{kj} is described as:

$$u_{kj}=s_{kj}u_{kj}^{\Sigma}, k=u,l \text{ and } j=a,b,c \tag{2}$$

The equivalent circuit for MMC during this stage has been proposed by using $s_{kj}*u_{kj}^{\Sigma}$ to represent the total SM voltage of each arm, which is shown in Fig. 2.

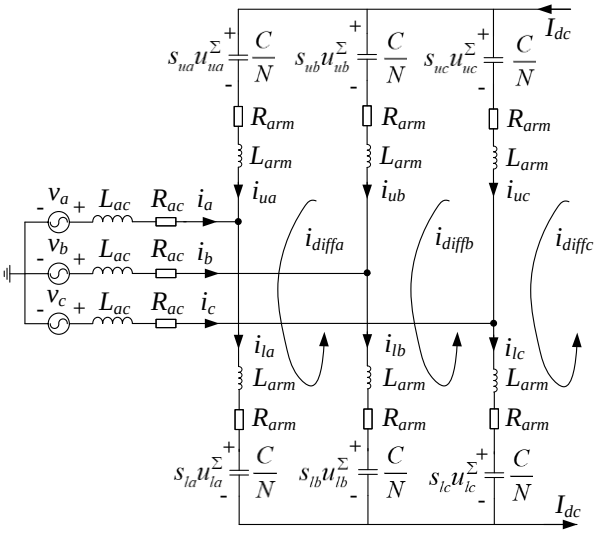

Fig. 2. The equivalent circuit of MMC under uncontrolled pre-charge process.

From Fig. 2, the currents flowing through the upper and lower arm of phase j are given as

$$\begin{cases} i_{uj}=-\dfrac{i_j}{2}+i_{diffj} \\ i_{lj}=\dfrac{i_j}{2}+i_{diffj} \end{cases}, j=a,b,c \tag{3}$$

where i_{diffj} is the difference current of phase j, i_{diffj}=(i_{uj}+i_{lj})/2, j=a, b, c.

The total capacitor voltage of the upper and lower arm are defined as:

$$\begin{cases} \dfrac{du_{uj}^{\Sigma}}{dt} = \dfrac{N}{C} s_{uj} i_{uj} \\ \dfrac{du_{lj}^{\Sigma}}{dt} = \dfrac{N}{C} s_{lj} i_{lj} \end{cases}, j = a,b,c \tag{4}$$

According to Fig. 2, the circuit equations can be derived following the Kirchhoff's voltage law (KVL). For the upper arm of phase-*a* and phase-*b*:

$$-v_a + L_{ac}\frac{di_a}{dt} + R_{ac}i_a - L_{arm}\frac{di_{ua}}{dt} - R_{arm}i_{ua} - s_{ua}u_{ua}^{\Sigma} + s_{ub}u_{ub}^{\Sigma} + R_{arm}i_{ub} + L_{arm}\frac{di_{ub}}{dt} - L_{ac}\frac{di_b}{dt} - R_{ac}i_b + v_b = 0 \tag{5}$$

For the lower arm of phase-*a* and phase-*b*:

$$-v_a + L_{ac}\frac{di_a}{dt} + R_{ac}i_a + L_{arm}\frac{di_{la}}{dt} + R_{arm}i_{la} + s_{la}u_{la}^{\Sigma} - s_{lb}u_{lb}^{\Sigma} - R_{arm}i_{lb} - L_{arm}\frac{di_{lb}}{dt} - L_{ac}\frac{di_b}{dt} - R_{ac}i_b + v_b = 0 \tag{6}$$

Subtracting (6) from (5), the differential equation of the difference current of phase-*a* and phase-*b* is expressed as

$$\frac{di_{diffa}}{dt} - \frac{di_{diffb}}{dt} = \frac{1}{2L_{arm}}\left[-2R_{arm}(i_{diffa} - i_{diffb}) - (s_{ua}u_{ua}^{\Sigma} + s_{la}u_{la}^{\Sigma}) + (s_{ub}u_{ub}^{\Sigma} + s_{lb}u_{lb}^{\Sigma})\right] \tag{7}$$

For the upper and lower arm of phase-*b* and phase-*c*, the differential equation of the difference current is derived as

$$\frac{di_{diffb}}{dt} - \frac{di_{diffc}}{dt} = \frac{1}{2L_{arm}}\left[-2R_{arm}(i_{diffb} - i_{diffc}) - (s_{ub}u_{ub}^{\Sigma} + s_{lb}u_{lb}^{\Sigma}) + (s_{uc}u_{uc}^{\Sigma} + s_{lc}u_{lc}^{\Sigma})\right] \tag{8}$$

From Fig. 2, the difference currents of MMC satisfy:

$$\frac{di_{diffa}}{dt} + \frac{di_{diffb}}{dt} + \frac{di_{diffc}}{dt} = \frac{dI_{dc}}{dt} \tag{9}$$

According to (7)-(9), the differential equations of difference current are

$$\begin{cases} \dfrac{di_{diffa}}{dt} = \dfrac{dI_{dc}}{3dt} + \dfrac{1}{6L_{arm}}\left[-2R_{arm}\left(2i_{diffa} - i_{diffb} - i_{diffc}\right) - 2(s_{ua}u_{ua}^{\Sigma} + s_{la}u_{la}^{\Sigma}) + (s_{ub}u_{ub}^{\Sigma} + s_{lb}u_{lb}^{\Sigma}) + (s_{uc}u_{uc}^{\Sigma} + s_{lc}u_{lc}^{\Sigma})\right] \\ \dfrac{di_{diffb}}{dt} = \dfrac{dI_{dc}}{3dt} + \dfrac{1}{6L_{arm}}\left[-2R_{arm}\left(2i_{diffb} - i_{diffa} - i_{diffc}\right) - 2(s_{ub}u_{ub}^{\Sigma} + s_{lb}u_{lb}^{\Sigma}) + (s_{ua}u_{ua}^{\Sigma} + s_{la}u_{la}^{\Sigma}) + (s_{uc}u_{uc}^{\Sigma} + s_{lc}u_{lc}^{\Sigma})\right] \\ \dfrac{di_{diffc}}{dt} = \dfrac{dI_{dc}}{3dt} + \dfrac{1}{6L_{arm}}\left[-2R_{arm}\left(2i_{diffc} - i_{diffa} - i_{diffb}\right) - 2(s_{uc}u_{uc}^{\Sigma} + s_{lc}u_{lc}^{\Sigma}) + (s_{ua}u_{ua}^{\Sigma} + s_{la}u_{la}^{\Sigma}) + (s_{ub}u_{ub}^{\Sigma} + s_{lb}u_{lb}^{\Sigma})\right] \end{cases} \tag{10}$$

Therefore, the MMC model under uncontrolled pre-charge process can be modeled by continuous updating the state variables by solving the differential equations (4) and (10).

The controlled pre-charge process follows the uncontrolled pre-charge process and the MMC converter is deblocked. The insertion index in the upper and lower arm of phase *j* n_{uj} and n_{lj} are determined by modulation signal m_j:

$$\begin{cases} n_{uj} = \dfrac{1 - m_j}{2} \\ n_{lj} = \dfrac{1 + m_j}{2} \end{cases}, j = a,b,c \tag{11}$$

The total SM voltage of in the *k* arm of phase *j* u_{kj} is described as:

$$u_{kj} = n_{kj}u_{kj}^{\Sigma}, k = u,l \text{ and } j = a,b,c \tag{12}$$

The proposed AVM for MMC under controlled charge process is obtained by replacing s_{kj} with n_{kj} in (4) and (10):

$$\begin{cases} \dfrac{du_{uj}^{\Sigma}}{dt} = \dfrac{N}{C} n_{uj} i_{uj} \\ \dfrac{du_{lj}^{\Sigma}}{dt} = \dfrac{N}{C} n_{lj} i_{lj} \end{cases}, j = a,b,c \tag{13}$$

$$\begin{cases} \dfrac{di_{diffa}}{dt} = \dfrac{dI_{dc}}{3dt} + \dfrac{1}{6L_{arm}}\left[-2R_{arm}\left(2i_{diffa} - i_{diffb} - i_{diffc}\right) - 2(n_{ua}u_{ua}^{\Sigma} + n_{la}u_{la}^{\Sigma}) + (n_{ui}u_{ui}^{\Sigma} + n_{li}u_{li}^{\Sigma}) + (n_{ui}u_{ui}^{\Sigma} + n_{li}u_{li}^{\Sigma})\right] \\ \dfrac{di_{diffb}}{dt} = \dfrac{dI_{dc}}{3dt} + \dfrac{1}{6L_{arm}}\left[-2R_{arm}\left(2i_{diffb} - i_{diffa} - i_{diffc}\right) - 2(n_{ub}u_{ub}^{\Sigma} + n_{lb}u_{lb}^{\Sigma}) + (n_{ua}u_{ua}^{\Sigma} + n_{la}u_{la}^{\Sigma}) + (n_{uc}u_{uc}^{\Sigma} + n_{lc}u_{lc}^{\Sigma})\right] \\ \dfrac{di_{diffc}}{dt} = \dfrac{dI_{dc}}{3dt} + \dfrac{1}{6L_{arm}}\left[-2R_{arm}\left(2i_{diffc} - i_{diffa} - i_{diffb}\right) - 2(n_{uc}u_{uc}^{\Sigma} + n_{lc}u_{lc}^{\Sigma}) + (n_{ua}u_{ua}^{\Sigma} + n_{la}u_{la}^{\Sigma}) + (n_{ub}u_{ub}^{\Sigma} + n_{lb}u_{lb}^{\Sigma})\right] \end{cases} \tag{14}$$

Therefore, the MMC model under controlled pre-charge process is modeled by continuous updating state variables value by solving the differential equations (13) and (14).

2.2 Normal Operation

In the normal operating condition, the MMC is also deblocked. The total SM voltage of each arm is still $n_{kj} * u_{kj}^{\Sigma}$. Therefore, the MMC model under normal operation is the same as the controlled pre-charge process, which is described as (13) and (14).

2.3 Model Configuration

The proposed model is shown in Fig. 3. The ac-side and dc-side of the MMC system are decoupled, represented by three-phase ac controlled voltage source e_j and a dc controlled voltage source U_{dc}:

$$\begin{cases} e_j = \dfrac{u_{lj} - u_{uj}}{2} \\ U_{dc} = \dfrac{\sum\limits_{j=a,b,c}(u_{uj} + u_{lj})}{3} \end{cases}, j = a,b,c \tag{15}$$

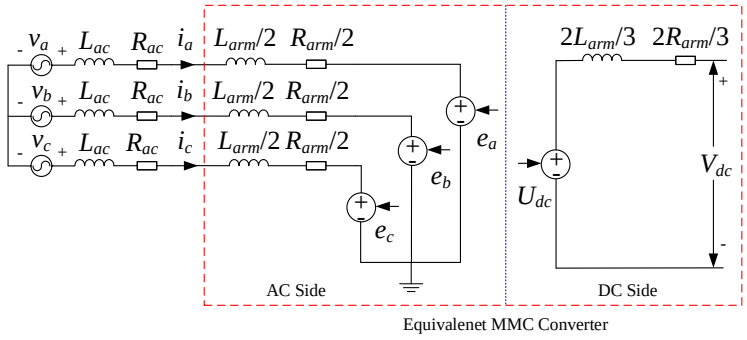

Equivalenet MMC Converter

Fig. 3. The proposed AVM for MMC system.

3 Model Validation

The performance of the proposed complete AVM is compared with detailed IGBT-based MMC-HVDC back to back system under different operation states in PSCAD/EMTDC. The schematic diagram of the simulation system is shown in Fig. 4.

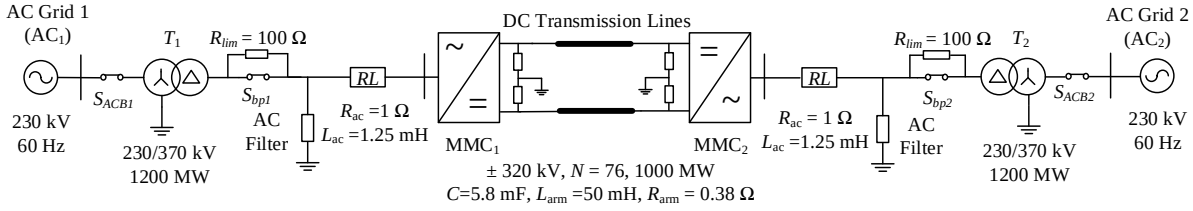

Fig. 4. The schematic diagram of the two terminals MMC-HVDC system.

The simulation system shown in Fig. 4 includes two MMCs, MMC_1 and MMC_2. Both converters are implemented with outer-loop voltage/power control and inner loop current control. The outer loop control for MMC_1 is dc voltage/ac voltage control while active power/ac voltage control for MMC_2. The control diagram of MMC_1 and MMC_2 are shown in Fig. 5(a) and (b), respectively. The time-step

in simulation is 10 μs. The proposed MMC model can be used to design the controller. A circulating current suppression control (CCSC) is applied in both side converters, and the control diagram is shown in Fig. 6.

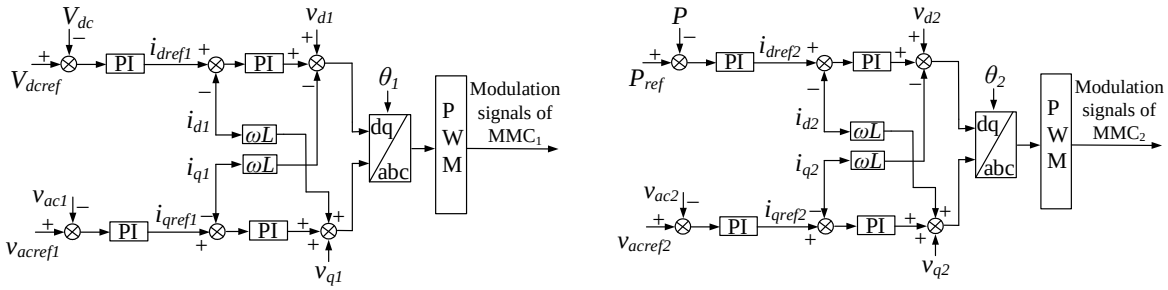

(a) The control schematic of MMC$_1$ (b) The control schematic of MMC$_2$

Fig. 5. The control diagram of MMC-HVDC simulation system.

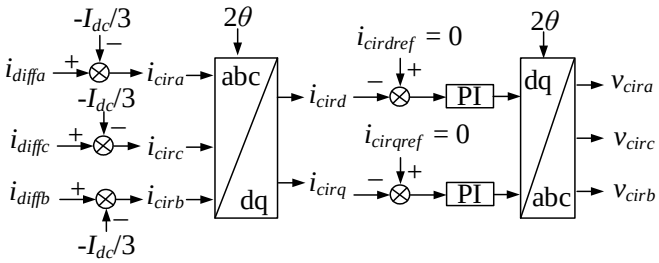

Fig. 6. The control diagram of CCSC.

3.1 Startup process

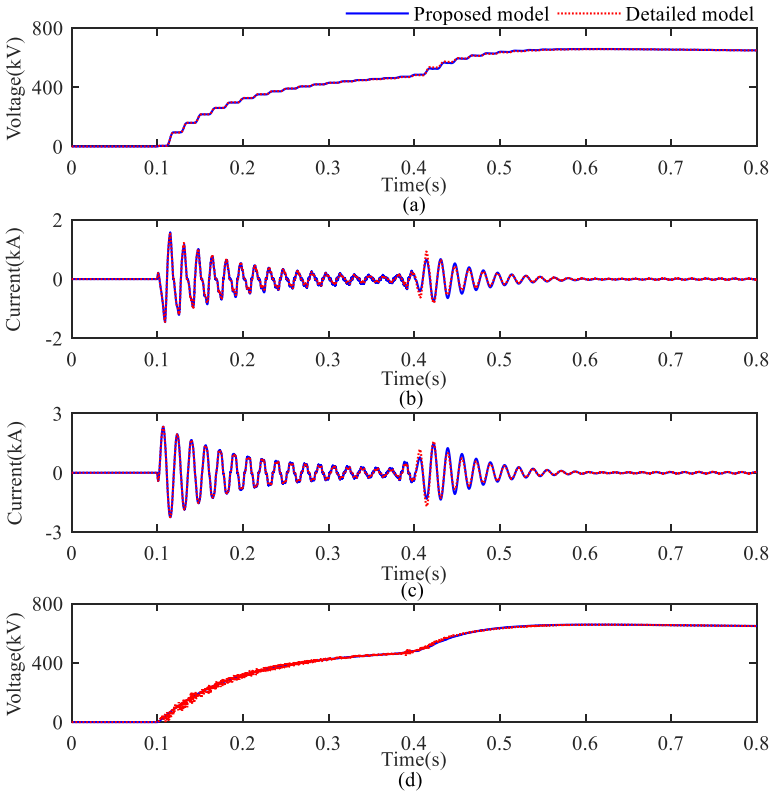

Fig. 7. MMC startup process. (a) Total capacitor voltage of MMC$_1$ phase-*a* upper arm. (b) Current of MMC$_1$ phase-*a* upper arm. (c) Phase-*a* current of T_1 secondary winding side. (d) DC-link voltage of MMC$_1$.

The response characteristics of the two models under the startup process are compared in Fig. 7. The total capacitor voltage and current in the upper arm of MMC$_1$ phase-*a* are shown in Fig. 7(a) and (b).

The phase-*a* current of transformer T_1 secondary winding side is shown in Fig. 7(c). Fig. 7(d) presents the dc-link voltage of MMC_1. The uncontrolled pre-charge process and controlled pre-charge process start at 0.1 s and 0.4 s, respectively. The simulation results illustrate that the proposed model can follow the detailed MMC model response accurately.

3.2 Steady-state operation

The steady-state responses of the two models are compared in Fig. 8. The total capacitor voltage and current in the upper arm of MMC_1 phase-*a* are shown in Fig. 8(a) and (b). The phase-*a* voltage and current of transformer T_1 secondary winding side are shown in Fig. 8(c) and (d). The simulation results show a perfect accordance between the proposed AVM and detailed MMC model during the steady-state operation.

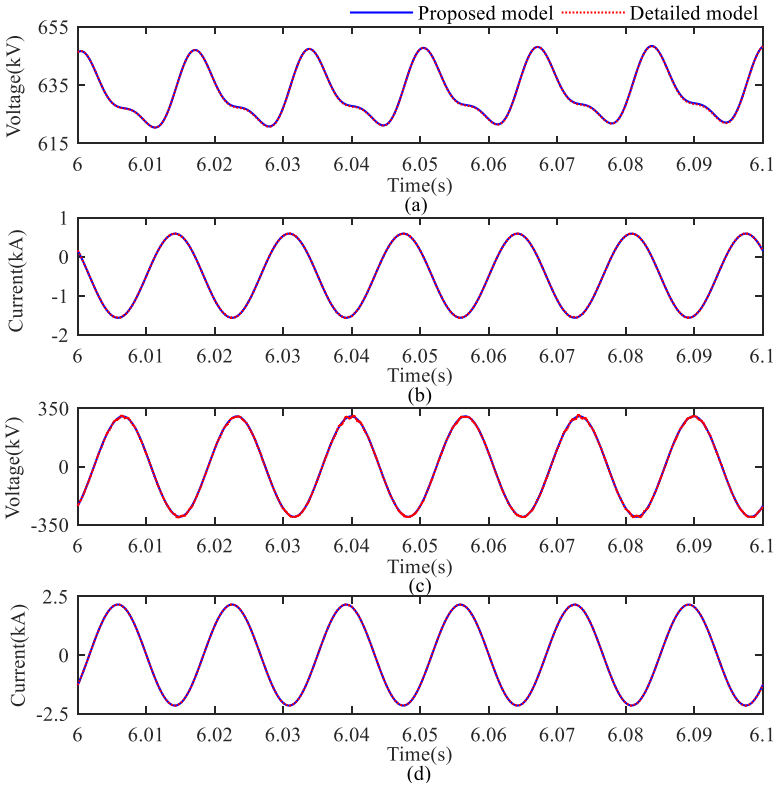

Fig. 8. MMC steady-state operation. (a) Total capacitor voltage of MMC_1 phase-*a* upper arm. (b) Current of MMC_1 phase-*a* upper arm. (c) Phase-*a* voltage of T_1 secondary winding side. (d) Phase-*a* current of T_1 secondary winding side.

3.3 CCSC

The CCSC is enabled at t = 4 s. The comparison results of the two models are presented in Fig. 9. Fig. 9(a) and (b) shows the total capacitor voltage and current in the upper arm of MMC_1 phase-*a*. The phase-*a* circulating current of MMC_1 and MMC_2 are shown in Fig. 9(c) and (d). It could be visualized from Fig. 9(c) and (d) that an obvious 2nd order (120 Hz) circulating current exists with a peak value of 0.1566 kA before 4 s. The circulating current of both models is eliminated after 4 s. The simulation results prove that the CCSC can suppress the circulating current effectively, and the proposed average value MMC model can replicate the dynamic performance of detailed model closely.

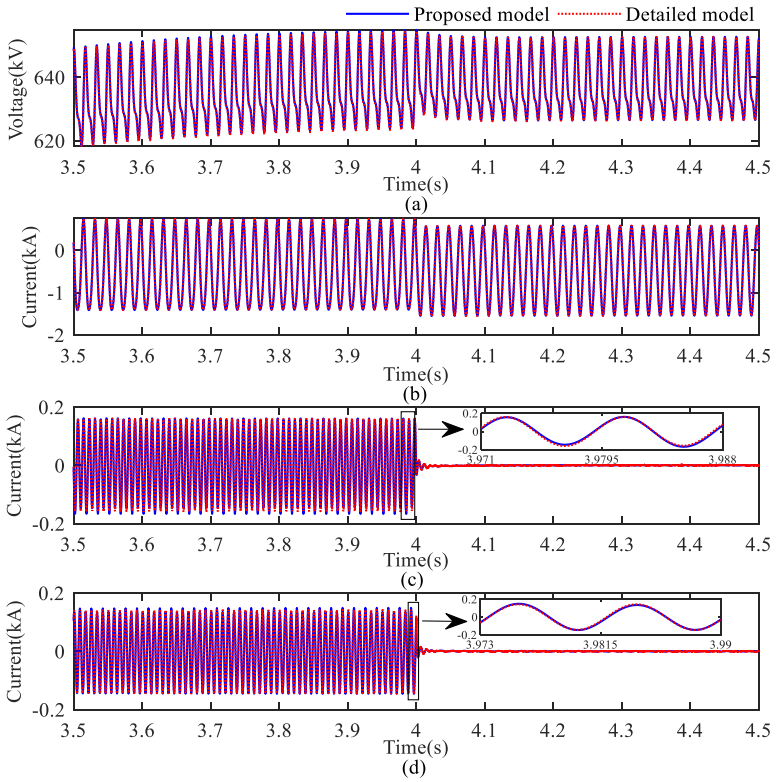

Fig. 9. CCSC of MMC. (a) Total capacitor voltage of MMC_1 phase-*a* upper arm. (b) Current of MMC_1 phase-*a* upper arm. (c) Circulating current of MMC_1 phase-*a*. (d) Circulating current of MMC_2 phase-*a*.

4 Conclusion

This paper analyses the operating conditions of MMC under the startup process and normal operation. The equivalent circuit of MMC under different operating scenarios is proposed to derive the ordinary differential equations of MMC internal variables afterwards. Furthermore, a complete AVM for MMC is established based on the ordinary differential equations. The proposed model is validated by the IGBTs-based MMC model in PSCAD/EMTDC under the startup process, steady-state operation and CCSC.

BIBLIOGRAPHY

[1] A. Lesnicar and R. Marquardt, “An innovative modular multilevel converter topology suitable for a wide power range,” in Proc. IEEE Power Tech. Conf., Bologna, Italy, Jun. 2003, pp. 1-6.

[2] Working Group B4.57 CIGRE, “Guide for the development of models for HVDC converters in a HVDC grid,” CIGRE Technical Brochure 604, Dec. 2014.

[3] Q. Song, W. Liu, X. Li, H. Rao, S. Xu, and L. Li, “A steady-state analysis method for a modular multilevel converters,” IEEE Trans. Power Electron., vol. 28, no. 8, pp. 3702-3713, Aug. 2013.

[4] F. Zhao, G. Xiao, and T. Zhao, “Accurate steady-state mathematical models of arm and line harmonic characteristics for modular multilevel converter,” IEEE Trans. Power Del., vol. 33, no. 3, pp. 1308-1318, Jun. 2018.

[5] J. Peralta, H. Saad, S. Dennetière, J. Mahseredjian, and S. Nguefeu, “Detailed and averaged models for a 401-level MMC–HVDC system,” IEEE Trans. Power Del., vol. 27, no. 3, pp. 1501-1508, Jul. 2012.

[6] H. Saad, et. al., “Modular multilevel converter models for electromagnetic transients,” IEEE Trans. Power Del., vol. 29, no. 3, pp. 1481-1489, Jun. 2014.

[7] J. Xu, A. M. Gole, and C. Zhao, “The use of averaged-value model of modular multilevel converter in DC grid,” IEEE Trans. Power Del., vol. 30, no. 2, pp. 519-528, Apr. 2015.

[8] A. Beddard, C. E. Sheridan, M. Barnes, and T. C. Green, “Improved accuracy average value models of modular multilevel converters,” IEEE Trans. Power Del., vol. 31, no. 5, pp. 2260-2269, Oct. 2016.